Faraday Discussions

Accepted Manuscript

Faraday Discussions

Royal Society of Chemistry

ROYAL SOCIETY OF CHEMISTRY

www.rsc.org/faraday_d

A Multifunctional Amphiphilic Polymer as a Platform for Surface-Functionalizing Metallic and Other Inorganic Nanostructures

Wentao Wang, Fadi Aldeek, Xin Ji, Birong Zeng, and Hedi Mattoussi

Department of Chemistry and Biochemistry, Florida State University, Tallahassee, FL 32306

Abstract

We designed a new set of polymer ligands that combine multiple metal-coordinating groups and short polyethylene glycol (PEG) moieties in the same structure. The ligand design relies on the controlled grafting of a large number of amine-terminated histamines and polyethylene glycol (PEG) short chains onto a poly(isobutylene-*alt*-maleic anhydride) backbone, via a one-step nucleophilic addition reaction. This addition reaction is highly efficient, can be carried out in organic media and does not require additional reagents. We show that when imidazoles groups are used the resulting polymer ligand can strongly ligate onto metal nanostructures such as nanoparticles and nanorods made of gold cores. The resulting polymer-coated nanoparticles and nanorods exhibit good colloidal stability to pH changes and added electrolytes. This constitutes a departure from the use of thiol-based ligand to coordinate on Au surfaces. The present chemical approach also opens up additional opportunities for design hydrophilic and reactive platforms where the polymer coating can be adjusted to various metal and metal oxide surfaces by simply modifying or combining the addition reaction with other metal coordinating groups. These could include iron oxide nanoparticles and semiconductor QDs. These polymer-capped nanoparticles and nanorods can be used to develop biologically-active platforms with potential use for drug delivery and sensing.

Email: mattoussi@chem.fsu.edu

Introduction

An effective integration of inorganic nanoparticles, such as those made of metal and metal oxide cores, within biological systems has the potential to provide novel hybrid platforms with unique photo-physical properties.[1,2] Such platforms can advance our understanding of various biologically challenging problems.[3-5] This, however, requires access to hydrophilic nanoparticles that are homogenously dispersed and reactive. It has been shown that the most successful route to prepare high quality nanocrystals of semiconductors, magnetic materials and even gold, with controllable size and high crystallinity, often rely on the thermal decomposition of metal precursors in hot surfactant solutions.[6-11] However, nanocrystals synthesized via pyrolysis of organometallic precursors are capped with hydrophobic ligands, which make them dispersible only in organic solvents. Consequently, integration within bio-inspired assemblies requires additional chemical manipulation and post growth surface modification to render the nanocrystals colloidally stable in buffer media and biocompatible.[3,12-15]

Use of amphiphilic polymers (e.g., block copolymers) and phospholipids to encapsulate the as-prepared hydrophobic nanoparticles within micelle-like structures has been employed by several groups to prepare various water-soluble NPs.[16-23] This route relies on the entropy-driven interdigitation between the hydrophobic segments of the polymers (or phospholipids) and the native cap. As a strategy, encapsulation is believed to better preserve the physical properties of the nanocrystals (e.g., optical or magnetic), because it maintains the native organic cap on the NP surfaces. It, however, tends to substantially increase the hydrodynamic size of the nanoparticles and may yield more than one nanocrystal per micelle,[16,23] which eventually limits their use in applications requiring small size probes. An alternative and more advantageous strategy relies on the removal of the hydrophobic cap and replacing it with bifunctional ligands: ligand exchange. These ligands present anchoring groups that coordinate onto the metal-rich surface of the nanocrystals along with hydrophilic moieties for promoting affinity interactions with the surrounding medium (i.e., buffer). These anchors interact with the metal surface via Lewis-base type coordination. This route can provide compact NPs and better colloidal stability in physiological conditions. When this strategy is applied using ligands with one anchoring group (i.e., monodentate ligands), the binding affinity to the NP surface is rather weak. This can

result in ligand desorption from the surfaces, which negatively affects the NP stability in biological media and/or at low concentrations. Furthermore, ligands with weak affinity can be easily displaced by biomolecules bearing amine and carboxylic functional groups, eventually promoting NP aggregation.[15] Multidentate ligands, in comparison, bind onto the inorganic nanocrystal surface, via multisite coordination, and can provide much stronger binding affinity. This drastically reduces the rate of ligand desorption compared to mono-dentate ligands, which improves the NP colloidal stability in biological media.[24-30]

In the present study, we design a new set of amphiphilic polymers that combine imidazole-to-metal coordination and hydrophilic PEG, as ligands that can promote the dispersion of Au nanoparticles and nanorods (as well as other inorganic nanocrystals) in buffer media. The polymer platform is synthesized via nucleophilic addition of several histamine groups and biocompatible hydrophilic moieties onto a poly(isobutylene-*alt*-maleic anhydride), PIMA, precursor.[30] This ligand design greatly benefits from the high efficiency of the addition reaction, while allowing simultaneous coupling of all desired groups in one step. We would also like to note that the histidine-coordination onto Au surfaces may be weaker than other groups (e.g., thiol-to-Au). However, this mode of ligand anchoring can be beneficial when competition to the ligands by other small molecules for binding to the Au surfaces are used to device a sensing scheme or drug delivery vehicles.[31]

Experimental Section

Materials. Poly(isobutylene-*alt*-maleic anhydride) (PIMA) (average Mw: ~ 6000 Da, 85%), poly(ethylene glycol) (average Mw: ~ 600 Da), poly(ethylene glycol) methyl ether (average Mw: ~ 750 Da), histamine (> 97.0%), hexadecyltrimethylammonium bromide (CTAB, > 98.0%), gold(III) chloride trihydrate (HAuCl$_4$·3H$_2$O, >99.9%), L-ascorbic acid (BioUltra, ≥ 99.5%), silver nitrate (AgNO$_3$, > 99%), sodium borohydride (NaBH$_4$, 99%), and hydrochloric acid (HCl, 37 wt. % in water), dimethylformamide, along with most of the chemicals used were purchased from Sigma Aldrich (St Louis, MO). Sodium oleate (purity > 97.0%) was purchased from Tokyo Chemical Industry Co, Ltd. Solvents were purchased from Sigma Aldrich (St Louis, MO). Column

purification chromatography was performed using silica gel (60 Å, 230 – 400 mesh from Bodman Industries, Aston, PA). Deuterated solvents used for H NMR experiments were purchased from Cambridge Isotope Laboratories (Andover, MA). Ultrapure water obtained from a Milli-Q Integral 5 system was used in all experiments. The precursors H_2N-PEG750-OCH_3 was synthesized in our laboratory following the procedures detailed in previous publications.[32]

The syntheses were carried out under N_2 passed through an O_2 scrubbing tower unless otherwise stated. Air sensitive materials were handled in a glovebox, and standard Schlenk techniques were used to handle of air-sensitive materials and reactions.

Instrumentation. ^{1}H NMR spectra were recorded using a 600 MHz spectrometer (Bruker SpectroSpin, Billerica, MA). Optical absorption data of various AuNP and AuNR dispersions were collected using an UV-Vis absorption spectrophotometer (UV 2450 model, Shimadzu, Columbia, MD) and UV-Vis-NIR spectrophotometer (Perkin Elmer Lambda 950). Fourier Transform Infrared (FT-IR) spectra were collected using an FT-IR spectrometer (Perkin Elmer Spectrum 100). Transmission electron microscopy (TEM) images were acquired using either a 200 kV JEOL-2010 instrument or a Philips FEI CM-120 microscope. Samples for TEM were prepared by drop casting the NP dispersion onto the holey carbon film on a fine mesh Cu grid (400 mesh). Dynamic light scattering measurements were carried out using an ALV/CGS-3 Compact Goniometer System (ALV-GmbH, Langen, Germany). This system is equipped with a HeNe laser (illumination at 632.8 nm), an ALV photon correlator and an avalanche photodiode for signal detection. Solvent evaporation was carried using a rotary evaporator R-215 (Buchi, New Castle, DE).

Synthesis of the His/PEG-PIMA Ligands. We briefly describe the synthesis of the histamine- and PEG-modified PIMA polymer where 50 % of the anhydride rings were targeted for reaction with histamines, while the other 50% were reacted with amine-PEG-OCH_3 moieties. In a typical reaction, 0.385 g of poly(isobutylene-alt-maleic anhydride) (PIMA, Mw ~ 6000 g/mol, 2.5 mmol monomer units) was dissolved in 10 mL of DMF and added into a 50 mL three-neck round-bottom flask equipped with a magnetic stirring bar and an addition funnel. The solution was purged with nitrogen and then heated up to 45 ˚C. Separately, histamine (0.139 g, 1.25 mmol)

and H_2N-PEG-OMe (0.995 g, 1.25 mmol) were dissolved in 4 mL of DMF. This solution mixture was added dropwise (via the addition funnel) to the PIMA solution above and the reaction mixture was further stirred at 45 ˚C for 8 – 10 hours (i.e., overnight). After removing the DMF under vacuum, 3 mL of chloroform was added, and the compound was purified on a silica column with chloroform as the eluent. The final product was gel-like compound, with a reaction yield of ~ 84%.

Growth of Gold Nanoparticles and Gold Nanorods. Three sets of Au nanostructures were prepared.

1) The first set is made of hydrophobic oleylamine-capped AuNPs (~ 5 nm in radius). The nanoparticles were synthesized by rapidly injecting $HAuCl_4$ precursors into a pre-heated surfactant solution, as reported by Swihart and coworkers.[33] Briefly, 5 mL oleylamine (OA) was refluxed at 150 °C in a 100 mL flask under argon. A mixture of 0.3 mmol of $HAuCl_4 \cdot 3H_2O$ in 1 mL oleylamine was rapidly injected into the above flask, and the mixture was further heated and annealed for 1.5 hours. One round of centrifugation/purification to remove unreacted precursor was applied, then the solution was diluted with hexane and stored until further use.

2) The second set is made of citrate-stabilized 13 nm diameter AuNPs, grown following procedure reported in the literature.[34,35] Briefly, 250 µL of 50 mM aqueous solution of $HAuCl_4 \cdot 3H_2O$ was mixed with 50 mL of water, and then stirred for ~ 1 min.   1 mL of 38.8 mM sodium citrate solution in water was added to the mixture. In parallel, 100 µL of 200 mM $NaBH_4$ was mixed with 900 µL of 38.8 mM sodium citrate solution, and rapidly injected in the above flask containing the Au precursor and ligands. The reaction mixture was stirred for an additional 2 hours, and then purified using a membrane filtration device; one round of concentration/dilution was applied.

3) The third set is made CTAB-coated Au nanorods (AuNRs with dimensions of 110 nm in length and 20 nm in diameter: 110 nm x 20 nm). These nanorods were prepared following the scheme initially developed by Murray and co-workers to grow gold nanorods using a seed solution and

a binary surfactant mixture (cetyltrimethulammonium, CTAB, and sodium oleate, NaOL).[36] The seed solution for the NR growth was prepared as follows: 5 mL of 0.5 mM HAuCl4 was mixed with 5 mL of 0.2 M CTAB solution in a 20 mL scintillation vial. 0.6 mL of fresh 0.01 M NaBH4 was diluted into 1 mL of water, and the mixture was then injected into the Au(III)-CTAB solution under vigorous stirring (1200 rpm). The solution color changed from yellow to brownish yellow and the stirring was stopped after 2 min. This seed solution was aged at room temperature for 30 min before use.

To prepare the growth solution required for the nanorods growth, 7.0 g (0.037 M in the final growth solution) of CTAB and 1.234 g of NaOL were dissolved in 250 mL of warm water (~ 50 °C) using a 1L Erlenmeyer flask. The solution was allowed to cool down to 30 °C and 24 mL of AgNO3 (4 mM) solution was added. The mixture was kept undisturbed at 30 °C for 15 min after which 250 mL of 1 mM HAuCl4 solution was added. The solution became colorless after 90 min of stirring (700 rpm). 3.6 mL of HCl (37 wt. % in water, 12.1 M) was then introduced to acidify the solution. After 15 min of slow stirring at 400 rpm, 1.25 mL of 0.064 M ascorbic acid (AA) was added and the solution was stirred vigorously for 30 s. Finally, 0.4 mL of seed solution was injected into the flask. The resulting mixture was stirred for 30 s and left undisturbed at 30°C for 12 h (overnight) to allow for growth and homogenization of the nanorods. The materials were isolated by centrifugation at 7,000 rpm for 30 min followed by removal of the supernatant.

Ligand Exchange with His/PEG-PIMA. Ligation with the above His/PEG-PIMA polymer ligand was applied to oleylamine-coated AuNPs, citrate-stabilized AuNPs and to CTAB/NaOL-coated AuNRs (referred to as CTAB-coated AuNRs).

a) Cap exchange of oleylamine-capped AuNPs. 400 µL of stock solution (~ 0.9 µM) was precipitated using ethanol and redispersed in 200 µL of chloroform. Then 15 mg of His/PEG-PIMA dissolved in 200 µL of chloroform was mixed with the AuNP solution. The vial was sealed with a rubber septum and the atmosphere was switched to nitrogen by applying 2 to 3 rounds of mild vacuum, followed by purging with nitrogen. The solution was then left stirring overnight while maintaining the temperature at 50 ˚C. The AuNPs were then precipitated by adding excess hexane and centrifuged for 5 min at 3700 RPM to provide a dark pellet. The clear

supernatant was discarded, and the pellet redissolved in 200 μL of chloroform, followed by precipitation using excess hexane. The turbid dispersion was centrifuged, the supernatant was discarded and the residual precipitate was dried under vacuum. This yielded a pellet which was easily dispersed by adding 500 μL of DI water. After sonication, the aqueous dispersion was filtered using a 0.45 μm disposable syringe filter, then excess free ligands were removed by applying 3 to 4 rounds of concentration/dilution using a centrifugal filtration device (Millipore, Mw cutoff = 50 kDa); 37000 rpm and 7 min were used.

b) *Cap exchange of citrate-stabilized AuNPs.* In a typical reaction, 4 mL of citrate-capped AuNPs (at a concentration of 14 nM) were added in a glass vial equipped with a magnetic stirring bar. In a separate vial, 2 mg of His/PEG-PIMA ligands were dispersed in 2 mL of 10 mM phosphate buffer (pH = 8.5). The ligand solution was added dropwise to the AuNP dispersion and stirred for 15 hours at room temperature. The cap exchanged AuNPs were then purified from free ligands by applying 3 rounds of concentration/dilution using a membrane filtration device as done above. The AuNPs were finally dispersed in DI water or buffers (if needed) and stored at 4 °C for later use.

C) *Ligation of CTAB/NaOL-coated AuNRs.* Ligation of the CTAB-coated nanorods was carried out using one phase ligand exchange in DI water. 120 μL of stock solution (2.82 nM, ε = 3.9 x 10^9 M^{-1} cm^{-1}) was purified by centrifugation (37000rpm, 10 min) to remove excess CTAB and sodium oleate. The concentrated AuNRs were then redispersed in 200 μL of DI water. 15 mg of ligands were dissolved in 200 μL of DI water and mixed with AuNR dispersion. The mixture was stirred at 50 ˚C overnight, then further diluted with 1 mL of DI water and sonicated for 2 min. The aqueous dispersion was filtered with a 0.45 μm disposable syringe filter, then excess free ligands were removed by applying 2 rounds of concentration/dilution using a centrifugal filtration device (Mw cutoff = 50 kDa) as described above.

Dynamic Light Scattering (DLS) Measurements. These measurements were applied to AuNPs only. Dynamic light scattering profiles were collected from dispersions of oleylamine-capped AuNPs in hexane, or citrate-stabilized AuNPs in DI water, and from the same NPs following

ligand-exchanged with His/PEG-PIMA and dispersed in buffer media (pH = 7.5). Data were collected using an ALV/CGS-3 Compact Goniometer System equipped with a He-Ne laser source (λ = 633 nm) and a variable delay time (multi-tau) ALV-7004 correlator (ALV-GmbH, Langen, Germany). All the dispersions were filtered through a 0.22 μm disposable filter (Millipore) before the scattered signal was collected. The scattered signal which consists of the average result of 3 acquisition periods of 10 seconds each was collected at angles varying between 60 and 120 degrees. The intensity count rates were maintained at ~ 150 – 300 Hz, achieved through appropriate control over the NP concentrations and density filters used. The resulting auto-correlation function, generated from the above scattered intensity profiles using the ALV correlator, was fitted to a cumulant series using ALV software. For every sample we verified that the measured hydrodynamic size (extracted from the Laplace transform of the auto-correlation function) is independent of the scattering angle, as anticipated.[37] The data on the hydrodynamic size reported here were collected at 90 degree scattering angle. To track possible changes in the NP size for a particular dispersion with time, the signal was collected and analyzed after different storage time periods.

NMR Characterization of the Hydrophilic AuNPs. We used pulsed field gradient water suppression ^{1}H-NMR to collect our spectra. This allowed collection of high signal-to-noise spectra using aqueous dispersions with relatively low concentration. ,The sample concentration used for our measurements were about 0.10 μM. Prior to spectra collection the solvent was switched from DI water to deuterium oxide (D_2O) by applying two rounds of concentration/dilution with 2 mL x 2. The final volume of AuNPs in D_2O was adjusted to 500 μL before NMR measurements. For instance, the ^{1}H-NMR spectra shown in Figure 4 were collected using His-PIMA-ligated-AuNPs at a concentration of 0.113 μM (and a volume of 500 μL) and averaged over 500 scans. The sample used for the surface ligand counting experiments was prepared following the same protocol, but 0.8 μL pyridine (9.93 μmol) was added to provide a standard to which the signature of the NPs were compared (i.e., the AuNP dispersion had a total volume of 500 μL and a concentration of 0.113 μM).

Results and Discussion

Ligand Synthesis. The polymer ligands used for the surface modification of AuNPs and AuNRs were prepared via nucleophilic addition reaction between poly(isobutylene-*alt*-maleic anhydride) (PIMA) and amine-containing molecules (here histamine and amine-PEG-methoxy). The synthetic design offers a few unique and advantageous features. The nucleophilic addition between anhydride rings and amine groups is highly efficient and can be carried out without the need for additional reagents, which simplifies the purification and characterization of the final products. In addition, the availability of several maleic anhydride rings per polymer chain permits a straightforward and controlled insertion of a large number of lateral groups with distinct chemical functionalities. This provides polymer ligands that simultaneously present several imidazole and PEG moieties, which increases the ligand coordination onto the NP surface, while promoting high affinity to water and reducing non-specific interactions. This synthetic design was successfully applied to prepare multi-dopamine-based ligands to functionalize magnetic nanoparticles.[30]

Figure 1 shows a schematic representation of the synthetic approach we used to prepare the His- PIMA-PEG ligand. Typically, we used a molar amount of aminated molecules (histamine and amine-PEG moieties) that was equal to the molar concentration of maleic anhydrides presented on the PIMA chains. In this study we introduced a 50:50 molar mixture of histamine and H_2N-PEG-OMe, but that ratios can be easily varied to tune the final composition of the polymer ligand. Overall, these conditions are expected to introduce a total of ~ 20 imidazoles and ~20 PEG moieties; it also frees ~ 40 carboxyl groups along the polymer chain.

The His- and PEG-modified PIMA polymer was characterized using ^{1}H NMR spectroscopy. The spectrum in Figure 1 shows two clearly defined peaks at 6.8 and 7.6 ppm, characteristic of the protons in the imidazole ring. Additional signatures include a strong peak at ~ 3.5 ppm and a sharp peak at ~ 3.23 ppm, which can be attributed to the protons in the PEG segments and the terminal methoxy protons, respectively, while a broad peak at ~ 0.9 ppm is attributed to the protons of the methyl groups in the polymer chain. The degree of grafting is estimated by

comparing the relative signal integrations of the 2 protons from the imidazole ring ($\delta \sim 6.8$ and 7.6 ppm, corresponding to 16.7 H and 15.9 H, respectively), the 3 protons from the methoxy group of the PEG moieties ($\delta \sim 3.23$, 57.9 H), and the protons of the two methyl repeat units of the PIMA chain ($\delta \sim 0.9$, 234 H). For the polymer compound above we measured $\sim 16 - 17$ imidazoles and ~ 19 PEG moieties per PIMA chain; such values are in agreement with the anticipated ones based on the nominal number of maleic anhydride rings per polymer chain, and the fact that the histamine-to-maleic anhydride and PEG-to-maleic anhydride molar ratios used in the addition reaction were 0.5.

Ligand Exchange. The hydrophobic NPs capped with oleylamine, with average radius R_0 of 5 nm (extracted from TEM, as shown in Figure 2), were synthesized using thermolysis of gold precursors, as reported previously.[33] The TEM images indicate that these nanoparticles are spherical with uniform cores and reduced size distribution. The nanoparticles were ligated with His/PEG-PIMA by mixing the polymer with the oleylamine capped-AuNPs in chloroform and stirring overnight at 50 ˚C, followed by purification. The nanoparticles capped with the new ligands were readily dispersible in water. An additional purification step to remove excess free ligands and solubilized oleic acid was carried out using a membrane filtration device (see Experimental Section). Figure 2A shows schematically the ligation and phase transfer of an oleylamine-AuNP using His/PEG-PIMA ligand. The white light images of AuNPs dispersed in immiscible phases made of hexane and water shows that oleylamine-capped AuNPs are limited to the hexane phase, but following ligand exchange with His/PEG-PIMA the NPs are homogeneously transferred to water (Figure 2B).

Characterization of the Hydrophilic AuNPs

1)   Optical Characterization. Figure 2C shows the absorption spectra of the AuNPs before and after ligand exchange with His/PEG-PIMA. The spectrum of AuNPs capped with His/PEG-PIMA-AuNPs dispersed in DI water is nearly identical to that collected from NPs capped with oleylamine dispersed in hexane. This indicates that the presence of the imidazoles in the polymer ligand indeed promote ligation of the NPs with no measurable deterioration or etching of the inorganic cores.

2) *Dynamic Light Scattering Measurements.* Figure 3A shows representative plots of the autocorrelation function collected from oleylamine-AuNPs diluted in hexane (blue symbols) and His/PEG-PIMA-capped AuNPs in water (red symbols). Data show that ligand exchange with the polymer ligands slightly increases the hydrodynamic size of the NPs, as indicated by the faster decay of the correlation function (slope in Figure 3B) measured for His/PEG-PIMA-AuNPs compared with oleylamine- AuNPs.[37] Plots of the intensity *vs* hydrodynamic size histograms extracted from the Laplace Transform of the autocorrelation function collected for both sets of NP dispersions are shown in Figure 3C. Overall, cap exchange with the polymer ligand yields dispersions of AuNPs with narrow size distribution, similar to what is measured for the hydrophobic dispersions (polydispersity index value, PDI, ≤ 0.1). The hydrodynamic radius (R_H) measured for oleylamine-AuNPs in toluene is 7.5 nm and increases to 11.2 nm for the AuNPs capped with His/PEG-PIMA dispersed in water (Figure 3b), a relatively small increase (~ 3-4 nm) compared to those measured for NP encapsulated with amphiphilic polymers reported in the literature.[38,39]

3) *^{1}H NMR Characterization.* The dispersion of AuNPs ligated with His/PEG-PIMA (in D_2O) was characterized using pulsed field gradient-based water suppression (of the peak at 4.7 ppm) ^{1}H-NMR spectroscopy. Figure 4A shows the ^{1}H-NMR spectrum of a dispersion of hydrophilic AuNPs ligated with His/PEG-PIMA, which is overall similar to the spectrum of ligands alone. The spectra show pronounced resonances at 3.24 ppm and 3.56 ppm corresponding to the methoxy groups and PEG moieties, while the broad peak at 0.84 ppm is attributed to the protons from PIMA backbone. The spectrum also indicates that the two disparate resonances at 6.8 and 7.6 ppm, characteristic of two protons on the imidazole ring, are shifted to 7.20 ppm along with much lower intensity compared with ligand alone (see Figure 1); this shift is due to the binding to AuNP surface and a change in its environment. In contrast, the NMR signals due to oleylamine ligands at 1.23 ppm, 1.98 ppm and 5.32 ppm in the spectrum (not shown here) collected from a solution of oleylamine capped AuNPs are essentially nonexistent in the sample of His/PEG-PIMA-capped nanocrystals. These results clearly indicate that cap exchange of oleylamine with His/PEG-PIMA is also driven by the imidazole coordination onto the surface of the AuNPs.

Quantifying the ligand Coverage on the NPs. To gain additional insights into the surface-to-ligand interactions, we used the above pulsed field gradient ^{1}H-NMR data to extract an estimate of the average number of His/PEG-PIMA ligand per AuNPs. This ligand density value was extracted by comparing the molar concentrations of the polymer ligands and that of the AuNPs in the medium. The molar concentration of the polymer was extracted by comparing the integrations of the methyl-proton of the polymer backbone (labeled as ***a***) and the α-proton of the pyridine standard (labeled as ***o***) shown in Figure 4B. The NP concentration was estimated from the Surface Plasmon Resonance (SPR) absorption data. Such analysis indicates that for a 5 nm radius AuNP there are about 30 polymeric ligands, which corresponds to ~ 600 His-anchors per AuNP.

Stability Test. The colloidal stability of aqueous dispersions of His/PEG-PIMA capped AuNPs (5 nm in radius) was tested in phosphate buffers at different pHs and in the presence of 1 M NaCl. The images shown in Figure 5A indicate that dispersions of His/PEG-PIMA-capped AuNPs are colloidally stable over the pH range from 3 to 13 and in the presence of 1 M NaCl for 1 month of storage. After 2 months, a visible color change of AuNP dispersion was observed at pH 3, indicating the microscopic aggregation of nanoparticles. Conversely, the dispersions stayed stable over the pH range 5 to 13 and in the presence of 1 M NaCl for at least 2 months of storage.

DLS measurements complemented the above data by allowing us to probe changes in the hydrodynamic size of the NPs with storage time under the various conditions shown in Figure 5B. Data indicate that a fixed hydrodynamic size was measured for the His/PEG-PIMA-capped NPs across the full pH range and in 1 M NaCl for the first 10-day period. Also, no change was measured for dispersions at pH 7-13 after 1 month of storage. However, sizable increases in R_H were measured for the dispersions at pH 3 and pH 5, though only dispersion at pH 3 exhibited macroscopic aggregation after 2 months of storage (Figure 5A). More precisely, the hydrodynamic size of the His/PEG-PIMA-NPs at pH 3 increased from ~ 11.4 nm to ~ 29.6 nm but to ~20 nm for dispersed at pH 5 after one month of storage. The weaker stability of

His/PEG-PIMA at lower pH may be attributed to a slow protonation of the imidazole groups, reducing the NP-to-ligand affinity and thus NP stability in acidic conditions.

Surface Modification of Citrate-Capped AuNPs and CTAB-Capped AuNRs. We further applied this polymer to surface-ligating citrate-capped AuNPs and CTAB-capped AuNRs. Figure 6A shows the absorption spectra of citrate-capped AuNPs (~ 6.5 nm in radius) before and after ligand exchange with His/PEG-PIMA. The spectra are essentially unchanged after ligation with His/PEG-PIMA. The hydrodynamic radius of His/PEG-PIMA-AuNP is about 15.0 nm, which is slightly larger than that measured for citrate- AuNP (~ 13.4 nm). This result confirms the compact coating provided by the multidentate polymer ligands. The hydrodynamic size for His/PEG-PIMA-AuNP dispersions was unchanged over the pH range 3 - 13 for 10 days. After ~ 1 month macroscopic aggregation was observed for dispersions at pH 3 and with excess salt; no reliable size measurements could be carried out for these conditions. At pH 5 R_H increased from 13 to 19 nm and a mild turbidity build up was observed. These may indicate that ligand exchange of citrate-stabilized AuNPs may not be as effective as was the case for oleylamine-AuNPs above. This may reflect a difference in the nature of the citrate capping (vs oleylamine coating) and the ligand exchange conditions used.

We further tested the ability of the His-PIMA polymer to ligate onto CTAB–coated AuNRs. For this CTAB-AuNRs (L x D = ~ 110 nm x 20 nm) were mixed with His/PEG-PIMA in DI water with mild heating for several hours. Figure 7A shows that the absorption spectra of the AuNRs before and after ligand exchange are essentially identical, with the clearly defined transverse and longitudinal Plasmon bands at 510 nm and 1050 nm, respectively, fully superposed for the two dispersions. The FT-IR spectra shown in Figure 7C confirm the ligand exchange of CTAB-capped AuNRs with the His/PEG-PIMA polymer, where the bands at ~ 1470 cm^{-1} (ascribed to the trimethylammonium groups of CTAB) and ~ 1720 cm^{-1} (attributed to the carbonyl groups of NaOL) in the initial dispersions have disappeared, while a new strong peak at ~ 1100 cm^{-1} (due to the ether bonds of PEG chains) is measured in the spectrum of polymer-coated AuNRs.

Conclusion

We have developed a flexible amphiphilic polymer platform as a metal-coordinating ligands based on the imidazole motif. In particular, we exploited the high and specific reactivity of maleic anhydride towards amine-modified molecules via the nucleophilic addition reaction, and synthesized a set of imidazole- and polyethylene glycol-modified polymers starting with poly(maleic anhydride) precursor. This synthetic route further allows control over the number and nature of the coordinating and hydrophilic groups introduced in the polymer platform. We showed that imidazole-modified polymer can strongly ligate onto Au nanoparticle and Au nanorods, yielding hydrophilic metal platforms with good colloidal stability to pH changes and excess electrolytes in neutral and basic conditions. This polymer-coating of metal nanostructures based on the imidazole motif is greatly promising, due to the ubiquitous presence of imidazole-containing histidine in proteins expressed using bacterial vectors. These polymers can also be used to develop sensing and drug delivery platforms based on competition interactions. One idea could start with a drug modified imidazole-polymer immobilized on AuNPs or AuNRs. These platforms could be introduced in live cells, then allow thiol-containing reducing agents, abundant in the cytoplasm, to alter the polymer coating and trigger the release of the drug. An alternative delivery mechanism could use laser induced-heating of the metal platform and partial release of the drug bearing polymer in vivo.

Faraday Discussions Accepted Manuscript

References

(1)   Ghosh, P.; Han, G.; De, M.; Kim, C. K.; Rotello, V. M. *Adv Drug Deliver Rev* **2008**, *60*, 1307.

(2)   Michalet, X.; Pinaud, F.; Bentolila, L.; Tsay, J.; Doose, S.; Li, J.; Sundaresan, G.; Wu, A.; Gambhir, S.; Weiss, S. *Science* **2005**, *307*, 538

(3)   Mattoussi, H.; Palui, G.; Na, H. B. *Adv Drug Deliver Rev* **2012**, *64*, 138.

(4)   Biju, V.; Itoh, T.; Ishikawa, M. *Chemical Society Reviews* **2010**, *39*, 3031.

(5)   Alivisatos, P. *Nature Biotechnology* **2004**, *22*, 47.

(6)   Rockenberger, J.; Scher, E. C.; Alivisatos, A. P. *J Am Chem Soc* **1999**, *121*, 11595.

(7)   Park, J.; An, K. J.; Hwang, Y. S.; Park, J. G.; Noh, H. J.; Kim, J. Y.; Park, J. H.; Hwang, N. M.; Hyeon, T. *Nature Materials* **2004**, *3*, 891.

(8)   Sun, S. H.; Zeng, H.; Robinson, D. B.; Raoux, S.; Rice, P. M.; Wang, S. X.; Li, G. X. *J Am Chem Soc* **2004**, *126*, 273.

(9)   Yu, W. W.; Falkner, J. C.; Yavuz, C. T.; Colvin, V. L. *Chem Commun* **2004**, 2306.

(10) Jun, Y. W.; Huh, Y. M.; Choi, J. S.; Lee, J. H.; Song, H. T.; Kim, S.; Yoon, S.; Kim, K. S.; Shin, J. S.; Suh, J. S.; Cheon, J. *J Am Chem Soc* **2005**, *127*, 5732.

(11) Reiss, P.; Bleuse, J.; Pron, A. *Nano Lett* **2002**, *2*, 781.

(12) Jun, Y. W.; Lee, J. H.; Cheon, J. *Angewandte Chemie-International Edition* **2008**, *47*, 5122.

(13) Zhang, F.; Lees, E.; Amin, F.; Gil, P. R.; Yang, F.; Mulvaney, P.; Parak, W. J. *Small* **2011**, *7*, 3113.

(14) Mout, R.; Moyano, D. F.; Rana, S.; Rotello, V. M. *Chem Soc Rev* **2012**, *41*, 2539.

(15) Ling, D.; Hyeon, T. *Small* **2013**, *9*, 1450.

(16) Kim, B. S.; Qiu, J. M.; Wang, J. P.; Taton, T. A. *Nano Lett* **2005**, *5*, 1987.

(17) Tromsdorf, U. I.; Bigall, N. C.; Kaul, M. G.; Bruns, O. T.; Nikolic, M. S.; Mollwitz, B.; Sperling, R. A.; Reimer, R.; Hohenberg, H.; Parak, W. J.; Forster, S.; Beisiegel, U.; Adam, G.; Weller, H. *Nano Lett* **2007**, *7*, 2422.

(18) Yu, W. W.; Chang, E.; Falkner, J. C.; Zhang, J. Y.; Al-Somali, A. M.; Sayes, C. M.; Johns, J.; Drezek, R.; Colvin, V. L. *J Am Chem Soc* **2007**, *129*, 2871.

(19) Lin, C. A.; Sperling, R. A.; Li, J. K.; Yang, T. Y.; Li, P. Y.; Zanella, M.; Chang, W. H.; Parak, W. J. *Small* **2008**, *4*, 334.

(20) Pellegrino, T.; Manna, L.; Kudera, S.; Liedl, T.; Koktysh, D.; Rogach, A. L.; Keller, S.; Radler, J.; Natile, G.; Parak, W. J. *Nano Lett* **2004**, *4*, 703.

(21) Lees, E. E.; Nguyen, T. L.; Clayton, A. H. A.; Muir, B. W.; Mulvaney, P. *ACS nano* **2009**, *3*, 2049.

(22) Wu, X. Y.; Liu, H. J.; Liu, J. Q.; Haley, K. N.; Treadway, J. A.; Larson, J. P.; Ge, N. F.; Peale, F.; Bruchez, M. P. *Nat Biotechnol* **2003**, *21*, 452.

(23) Mikhaylov, G.; Mikac, U.; Magaeva, A. A.; Itin, V. I.; Naiden, E. P.; Psakhye, I.; Babes, L.; Reinheckel, T.; Peters, C.; Zeiser, R.; Bogyo, M.; Turk, V.; Psakhye, S. G.; Turk, B.; Vasiljeva, O. *Nat Nanotechnol* **2011**, *6*, 594.

(24) Zhang, T. R.; Ge, J. P.; Hu, Y. X.; Yin, Y. D. *Nano Lett* **2007**, *7*, 3203.

(25) Shukoor, M. I.; Natalio, F.; Ksenofontov, V.; Tahir, M. N.; Eberhardt, M.; Theato, P.; Schroder, H. C.; Muller, W. E.; Tremel, W. *Small* **2007**, *3*, 1374.

(26) Liong, M.; Shao, H.; Haun, J. B.; Lee, H.; Weissleder, R. *Adv Mater* **2010**, *22*, 5168.

(27) Stewart, M. H.; Susumu, K.; Mei, B. C.; Medintz, I. L.; Delehanty, J. B.; Blanco-Canosa, J. B.; Dawson, P. E.; Mattoussi, H. *J Am Chem Soc* **2010**, *132*, 9804.

(28) Ling, D.; Park, W.; Park, Y. I.; Lee, N.; Li, F.; Song, C.; Yang, S. G.; Choi, S. H.; Na, K.; Hyeon, T. *Angew Chem Int Edit* **2011**, *50*, 11360.

(29) Na, H. B.; Palui, G.; Rosenberg, J. T.; Ji, X.; Grant, S. C.; Mattoussi, H. *ACS nano* **2012**, *6*, 389.

(30) Wang, W.; Ji, X.; Na, H. B.; Safi, M.; Smith, A.; Palui, G.; Perez, J. M.; Mattoussi, H. *Langmuir* **2014**.

(31) Aldeek, F.; Safi, M.; Zhan, N. Q.; Palui, G.; Mattoussi, H. *ACS Nano* **2013**, *7*, 10197.

(32) Mei, B. C.; Susumu, K.; Medintz, I. L.; Delehanty, J. B.; Mountziaris, T. J.; Mattoussi, H. *J Mater Chem* **2008**, *18*, 4949.

(33) Liu, S.; Chen, G. Y.; Prasad, P. N.; Swihart, M. T. *Chem Mater* **2011**, *23*, 4098.

(34) Brown, K. R.; Walter, D. G.; Natan, M. J. *Chem Mater* **2000**, *12*, 306.

(35) Tournebize, J.; Boudier, A.; Sapin-Minet, A.; Maincent, P.; Leroy, P.; Schneider, R. *ACS applied materials & interfaces* **2012**, *4*, 5790.

(36) Ye, X. C.; Zheng, C.; Chen, J.; Gao, Y. Z.; Murray, C. B. *Nano Lett* **2013**, *13*, 765.

(37) Pons, T.; Uyeda, H. T.; Medintz, I. L.; Mattoussi, H. *Journal of Physical Chemistry B* **2006**, *110*, 20308.

(38) Kang, Y. J.; Taton, T. A. *Macromolecules* **2005**, *38*, 6115.

(39) Li, W. K.; Liu, S. Q.; Deng, R. H.; Wang, J. Y.; Nie, Z. H.; Zhu, J. T. *Macromolecules* **2013**, *46*, 2282.
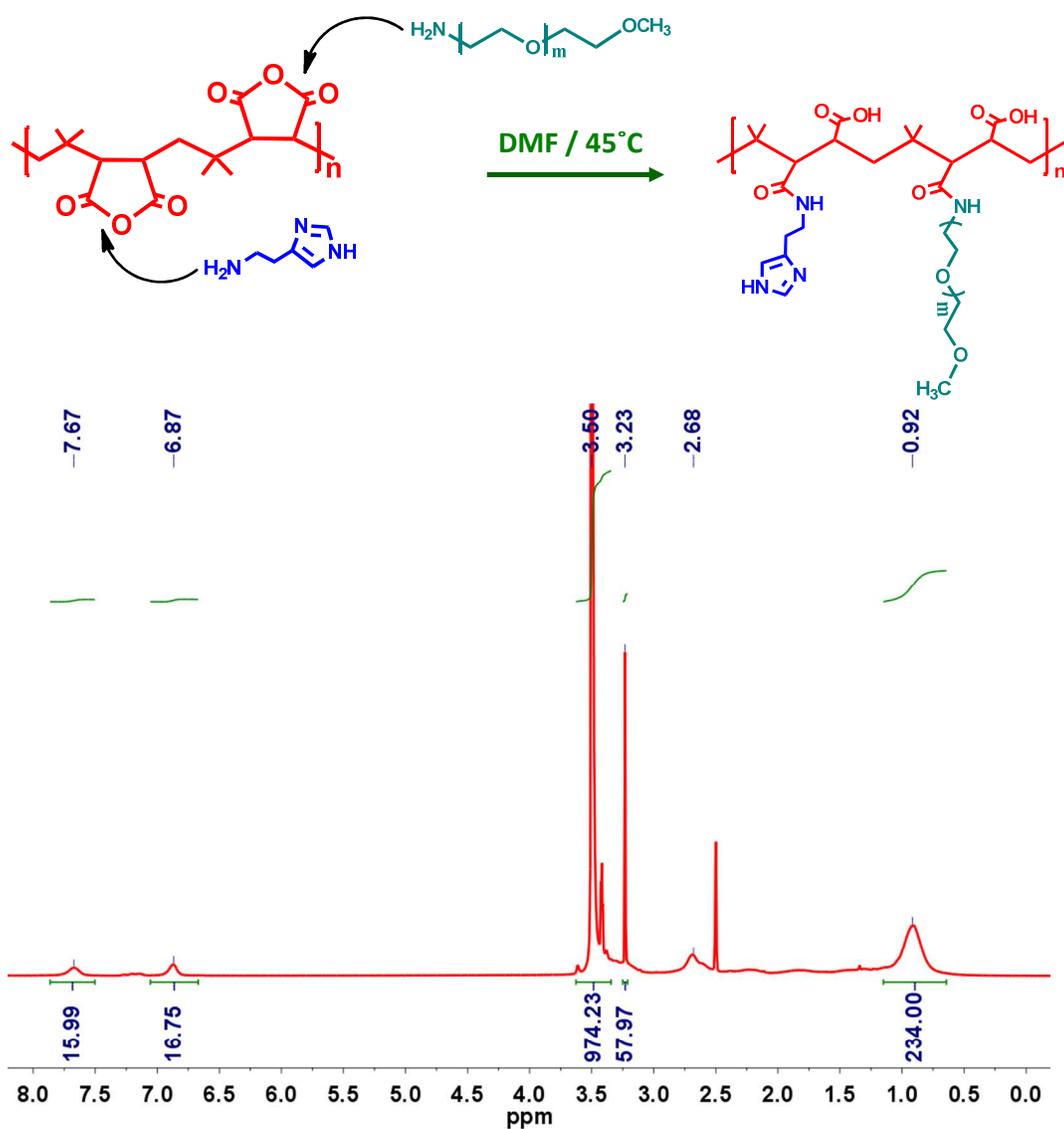
Figures and Captions

Ligand Design: His-PEG-PIMA

Figure 1: (top) Schematic representation of the nucleophilic addition reaction used to introduce both histamine groups and amine-modified PEG moieties along the same PIMA polymer chain. (bottom) ^{1}H NMR spectrum collected from a solution of His/PEG-PIMA ligand (made with 50:50 mixture of imidazole and PEGalong the PIMA backbone) dissolved in DMSO-d_6.
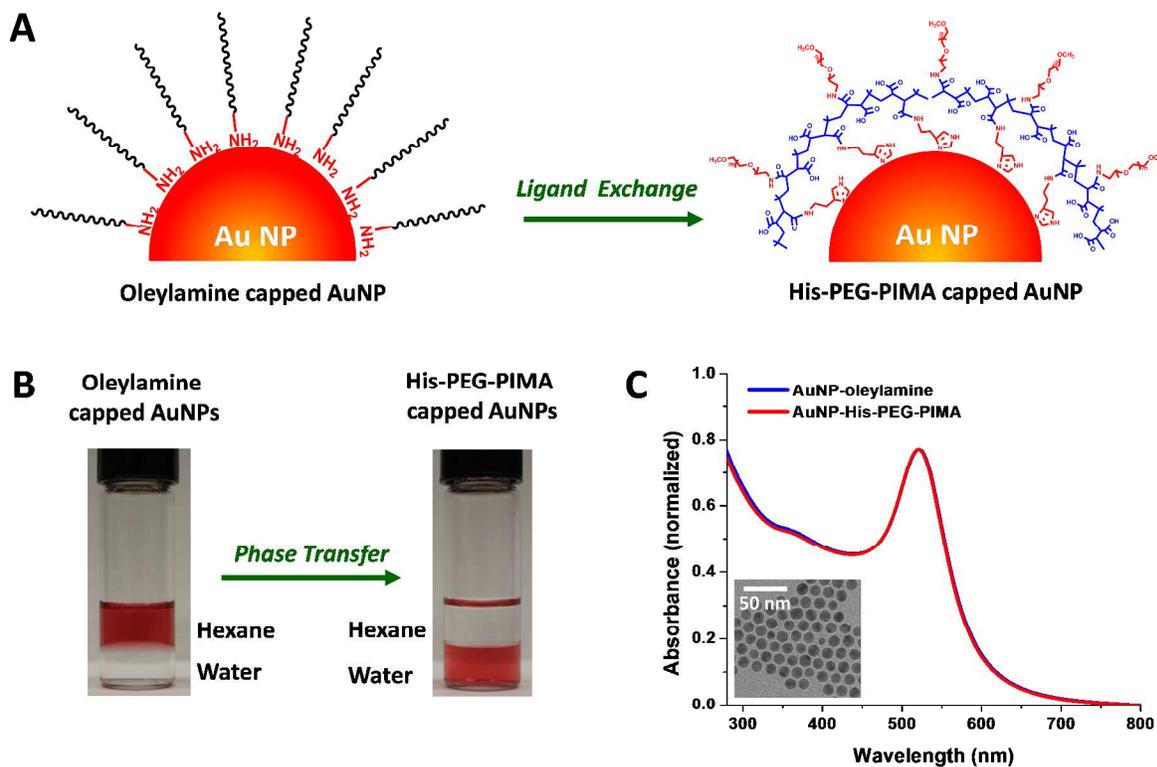
17

Figure 2. A) Schematics depiction of an oleylamine-capped AuNP (left) and the same NP following ligation with His/PEG-PIMA (right). B) White light images of a two-phase dispersion showing oleylamine-AuNPs dispersed in the hexane (top) phase and after ligand exchange with His/PEG-PIMA where the NPs are homogeneously dispersed in the water bottom phase. C) UV-Vis absorption spectra of dispersion of hydrophobic oleylamine-AuNPs in hexane and following phase transfer to water using His/PEG-PIMA polymer. Inset shows the TEM image of oleylamine-capped AuNPs (5 nm in radius).
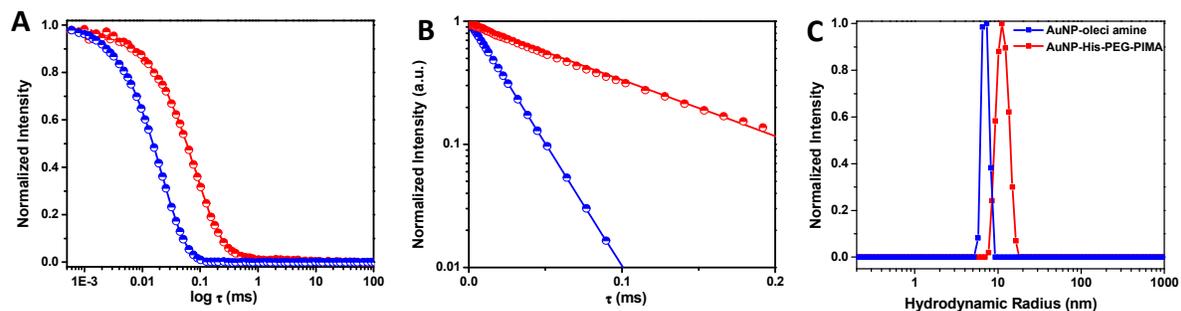
Figure 3. Representative plots of the autocorrelation function, $g^{(2)}$, collected from dispersions of 5 nm AuNPs before and after cap exchange with the His/PEG-PIMA; shown are: (A) $(g^{(2)})$ vs. ln (lag time, τ), and (B) ln $(g^{(2)})$ vs. lag time (τ). (C) Histograms showing the distribution of the intensity vs. hydrodynamic radius, extracted from the Laplace Transform of the intensity auto-correlation function from the above dispersions of oleylamine- and His/PEG-PIMA-capped AuNPs.

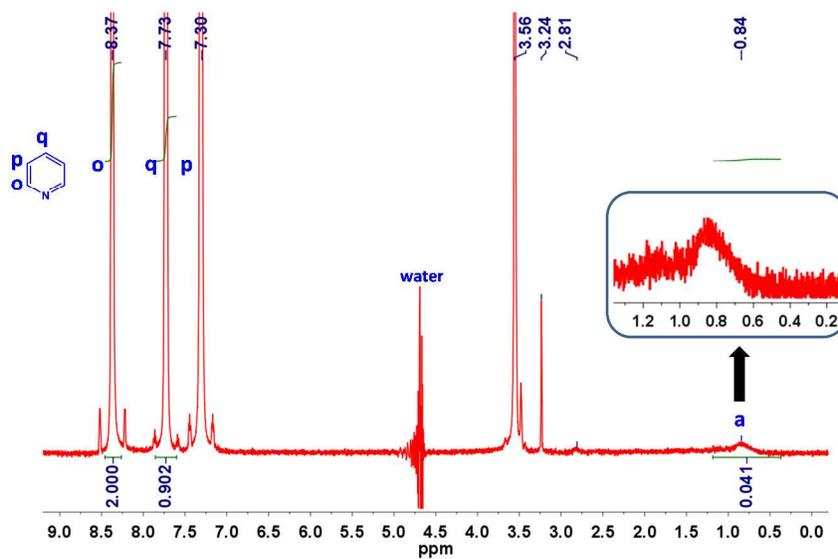**A: polymer-capped AuNP dispersion**
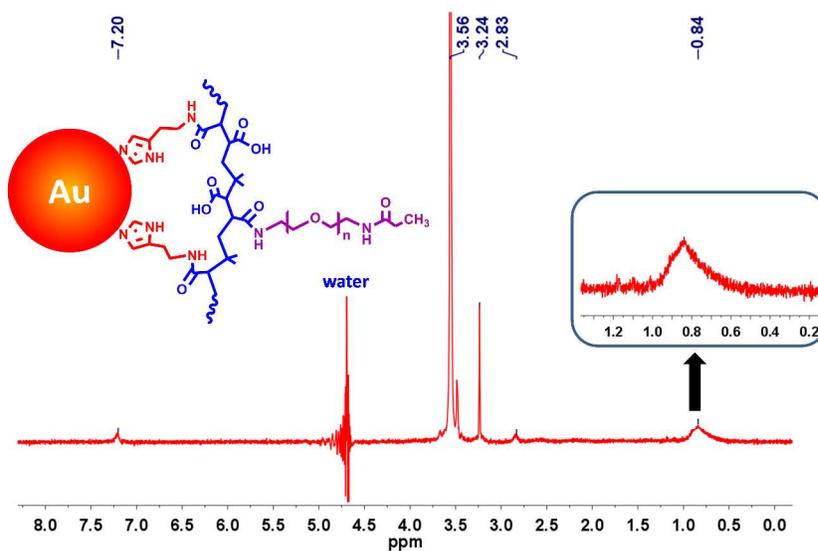
B: Calibration with pyridine

Figure 4: (A) ^{1}H-NMR spectrum of the hydrophilic His/PEG-PIMA-capped AuNPs. (B) ^{1}H-NMR spectrum of the His/PEG-PIMA polymer calibrated with a fixed amount of pyridine (used as a control).
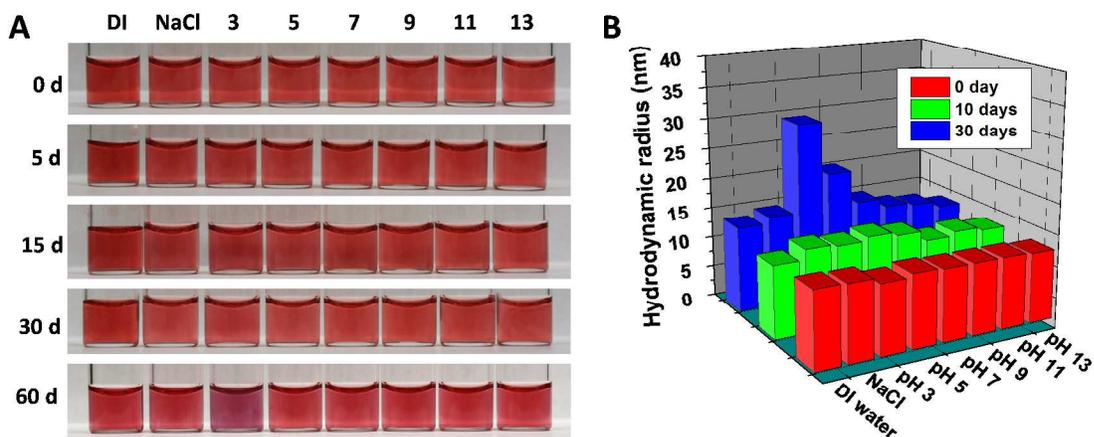
Figure 5: Colloidal stability tests: (A) AuNPs (5 nm) ligand exchanged with His/PEG-PIMA dispersed in phosphate buffer (20 mM) over the pH range from 3 to 13 and in the presence of 1 M NaCl; (B) Time-progression of the hydrodynamic radius measured from AuNP dispersions ligand exchanged with His/PEG-PIMA.
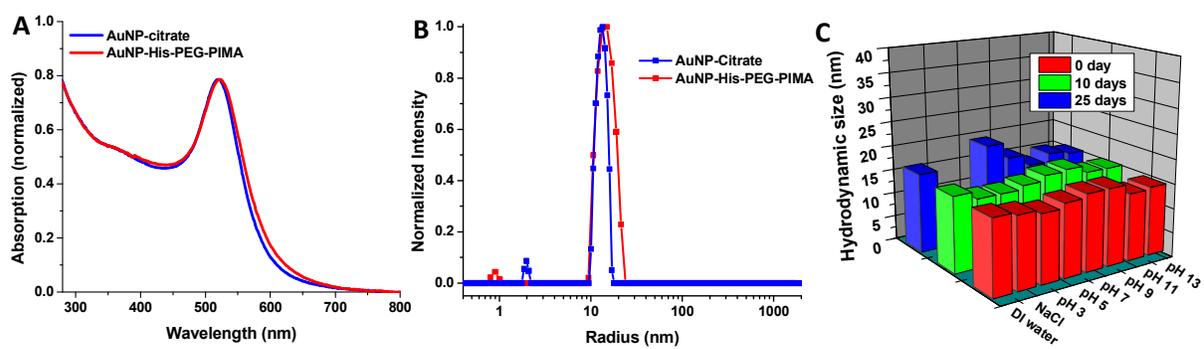
Figure 6. (A) UV-Vis absorption spectra collected from aqueous dispersions of 13 nm (diameter) citrate-stabilized AuNPs and following ligand exchange with His/PEG-PIMA. (B) Histograms showing the distribution of the intensity vs. hydrodynamic radius measured for the citrate-stabilized AuNPs and His/PEG-PIMA-AuNPs. (C) Time-progression of the hydrodynamic radius of His/PEG-PIMA-AuNPs (prepared by ligand exchange of citrate-AuNPs). Values at pH 3 and in the presence of 1 NaCl are not shown after for day 25, due to sample precipitation.
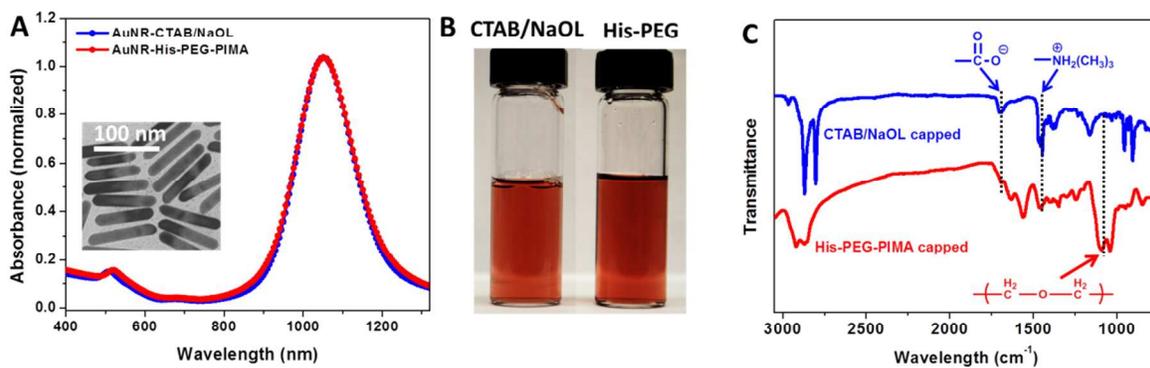
Figure 7. (A) UV-Vis-NIR absorption spectra of aqueous dispersion of AuNRs capped with CTAB/NaOL and after ligand exchange with His/PEG-PIMA; insert shows a TEM image of the NRs. (B) White light images of CTAB/NAOL capped AuNR dispersion and His/PEG-PIMA capped AuNR dispersion in water. (C) FT-IR spectra of CTAB/NaOL- and His/PEG-PIMA-capped AuNRs.